Journal of Magnetic Resonance 281 (2017) 188–198

Contents lists available at ScienceDirect

Journal of Magnetic Resonance

journal homepage: www.elsevier.com/locate/jmr

Obtaining sparse distributions in 2D inverse problems

A. Reci, A.J. Sederman *, L.F. Gladden

Department of Chemical Engineering and Biotechnology, University of Cambridge, Pembroke Street, Cambridge CB2 3RA, United Kingdom

ARTICLE INFO

Article history:
Received 1 April 2017
Revised 19 May 2017
Accepted 22 May 2017
Available online 25 May 2017

Keywords:
L_1 regularization
Inverse problems
2D NMR correlation experiments
2D inverse Laplace transformation

ABSTRACT

The mathematics of inverse problems has relevance across numerous estimation problems in science and engineering. L_1 regularization has attracted recent attention in reconstructing the system properties in the case of sparse inverse problems; i.e., when the true property sought is not adequately described by a continuous distribution, in particular in Compressed Sensing image reconstruction. In this work, we focus on the application of L_1 regularization to a class of inverse problems; relaxation-relaxation, T_1–T_2, and diffusion-relaxation, D–T_2, correlation experiments in NMR, which have found widespread applications in a number of areas including probing surface interactions in catalysis and characterizing fluid composition and pore structures in rocks. We introduce a robust algorithm for solving the L_1 regularization problem and provide a guide to implementing it, including the choice of the amount of regularization used and the assignment of error estimates. We then show experimentally that L_1 regularization has significant advantages over both the Non-Negative Least Squares (NNLS) algorithm and Tikhonov regularization. It is shown that the L_1 regularization algorithm stably recovers a distribution at a signal to noise ratio < 20 and that it resolves relaxation time constants and diffusion coefficients differing by as little as 10%. The enhanced resolving capability is used to measure the inter and intra particle concentrations of a mixture of hexane and dodecane present within porous silica beads immersed within a bulk liquid phase; neither NNLS nor Tikhonov regularization are able to provide this resolution. This experimental study shows that the approach enables discrimination between different chemical species when direct spectroscopic discrimination is impossible, and hence measurement of chemical composition within porous media, such as catalysts or rocks, is possible while still being stable to high levels of noise.

1. Introduction

In many applications, the properties of the system to be measured, referred to as the 'distribution', are distorted by a physical process or the measuring instrument itself. When the system properties and the physical process are known, it is easy to simulate what the acquired signal should be. This is called a forward problem. In contrast, recovering the system properties from knowledge of the acquired signal and the physical process is known as an inverse problem. Inverse problems occur in areas as diverse as quantum mechanics [1], molecular electrostatics [2], capillary filling [3], chemical reactions [4], electron ionisation [5] and Nuclear Magnetic Resonance (NMR) [6]. In this work, we focus on a particular class of inverse problems, spin–lattice relaxation - spin–spin relaxation, T_1–T_2, and diffusion – spin–spin relaxation, D–T_2, correlation experiments in NMR. 2D NMR experiments are increasingly used to characterise multi-component, multi-phase systems. In addition to well-established 2D and multi-dimensional NMR spectroscopy experiments [7], T_1–T_2 experiments are used in characterizing the pore structure of rocks [8], probing adsorbate–adsorbent interactions [9], and discriminating between tissues in medicine [10] and D–T_2 experiments have found application in characterizing fluids in porous media [11], in correlating D and T_2 with the viscosity of heavy oils [12], and in analysing the pore geometry in conjunction with Magnetic Resonance Imaging (MRI) [13].

Unlike forward problems, inverse problems are typically ill–conditioned. This means that small differences in the acquired signal from an experiment, caused by the random nature of noise or experimental error, can lead to significantly different reconstructed distributions. It follows that the reconstruction of distributions from ill-conditioned inverse problems has attracted much attention [14–21]. The simplest method of inversion is the Non-Negative Least Squares (NNLS) algorithm [14]. However, the problem with this approach is that it does not address the ill-conditioning issue and the reconstructed distribution is very sensitive to the noise in the acquired signal. This can result in an over–estimate or under–estimate of the number of peaks assigned to the resulting distribution which can, of course, lead to misinterpretation of the experimental data [22,23]. The most common

* Corresponding author.
E-mail address: ajs40@cam.ac.uk (A.J. Sederman).

http://dx.doi.org/10.1016/j.jmr.2017.05.010
1090-7807/

method of inversion is Tikhonov regularization [15] and successful algorithms have been developed to solve this regularized problem [16,17]. Tikhonov regularization addresses the ill–conditioning by imposing constraints to the reconstructed distribution. A distinguishing feature of this method is that the reconstructed distribution is smooth; *i.e.* there is a gradual transition from one feature to another. This method works well when the distribution is *a priori* known to be smooth and it has been successfully used in various applications [24–26]. However, due to the smoothness, features in the distribution which are close together cannot be resolved properly [6,27,28], and therefore the spectral resolution is low. When applied to distributions which are sparse, that is with only a few non-zero entries, the magnitude and spread of the features can be incorrectly estimated. If the features are close together, Tikhonov regularization will often not distinguish between them.

The emerging idea of Compressed Sensing [29] and its increasing exploitation in different areas [30–34] has introduced a new form of regularization which is based on an L_1 minimization problem. The principle idea of Compressed Sensing is the reduction in the number of samples needed to reconstruct a distribution which is sparse in some domain. However, the form of regularization that it uses, which from now on will be referred to as L_1 regularization, also promotes the sparsity of the distribution in a particular domain. For distributions which are expected to be sparse, the enforcement of sparsity is synonymous with an increase in the spectral resolution of the reconstructed distribution. In addition to the potential for higher spectral resolution, an L_1 regularized problem is also expected to be more stable to noise than the non-regularized version. Indeed, L_1 regularization has been used in denoising sparse signals [35]. The potential of L_1 regularization to increase spectral resolution in inverse problems, while being stable to high levels of noise, has only recently begun to be realised [32,36–38]. Indeed, the recent work of Benjamini and Basser [36,37] showed how L_1 regularization could be used as a tool to reduce the amount of data required for 2D NMR relaxation–diffusion data reconstruction, but did not focus on the attributes of L_1 regularization in reconstructing sparse distributions and its stability to noise. One reason for the late arrival of L_1 regularization in applications to inverse problems in science and engineering is that the algorithms that have been developed to solve the L_1 regularized problem [39–41] are only suited to inverse problems where the signal and the distribution are related by transforms which are computationally easy to invert, such as the Fourier transform or the identity transform. However, in many inverse problems, the signal and the distribution are related by transforms which are harder to invert, such as exponential decay functions in the case of 2D NMR correlation experiments.

In this manuscript, an algorithm is introduced which is robust in reconstructing distributions from ill-conditioned, L_1 regularized inverse problems. A guide to the implementation of the L_1 minimization algorithm is given, including the choice of the regularization parameter and the assignment of error estimates. The algorithm is demonstrated experimentally by applying it to T_1–T_2 and D–T_2, correlation experiments, where the signal and the distribution are related by exponential decay functions. It is shown that the L_1 regularized inverse problem gives accurate results at signal-to-noise ratios (SNR) < 20. In contrast, the NNLS algorithm required SNR > 20 for the accurate discrimination of discrete components. Further, it is shown that when L_1 regularization is applied, chemical components with relaxation time constants and diffusion coefficients that differ from one another by as little as 10% can be distinguished. In contrast, Tikhonov regularization typically requires a factor 3 difference in relaxation constants or diffusion coefficients if the individual relaxation times or diffusion coefficients are to be identified [6].

While, in the present work, L_1 regularization and the algorithm proposed to solve the L_1 regularized inverse problems are applied to T_1–T_2 and D–T_2 NMR experiments, their application is not limited to these experiments. The approach is readily applied to other 2D NMR correlation experiments, such as T_2–T_2 [42,43] and D–D [44,45], as well as to the inverse problems which occur in areas other than NMR [1–5], as long as there is a prior knowledge that the true distribution is sparse. Of particular interest could be the application to D–δ, or Diffusion Ordered Spectroscopy (DOSY) [46] experiments, where δ stands for the chemical shift.

The paper is structured as follows: in Section 2 the mathematical formalism of the NNLS algorithm and Tikhonov regularization are presented, as well as the proposed L_1 regularization and its implementation. In Section 3 the materials and methods used are described, and a practical guide to implementing the L_1 minimization algorithm with an objective level of sparsity is given. Further, a method to assign error estimates is suggested. The experimental results for the application of the three inversion methods in the processing of 2D NMR correlation data are shown in Section 4. We investigate samples in which separation of components based on the 2D NMR signal is of increasing difficulty, with the most difficult being mixtures of hexane and dodecane imbibed within porous silica beads which remain immersed within the bulk liquid mixture; thereby forming a system in which discrimination of both chemical species existing in the bulk liquid state and within the porous medium is required. In this system, hexane and dodecane cannot be resolved spectroscopically neither in the bulk phase nor imbibed within the porous silica beads. Further, the similarity of relaxation time constants and diffusion coefficients of hexane and dodecane make it impossible to resolve these two components using the NNLS algorithm or Tikhonov regularization in 2D NMR correlation experiments. Resolving the individual diffusion coefficients and relaxation time constants in both the bulk liquid phase and within the porous medium, as well as quantifying the relative amount of each component in both phases, within the same experiment, is invaluable in understanding the behaviour of multiple chemical components inside catalysts [47] and rocks [48] *in situ*.

2. Mathematical treatment

2.1. Conventional inversion algorithms

This work will focus on inverse problems that can be written as:

$$\underline{S} = \underline{K}\,\underline{F} + \underline{E} \tag{1}$$

where $\underline{S}$ is the 2D signal matrix, $\underline{F}$ is the 2D distribution matrix to be found, $\underline{K}$ is the kernel matrix representing physical processes and $\underline{E}$ is a 2D unknown noise matrix, assumed to be inherent in the signal and of Gaussian distribution. By using the vectorized forms of $\underline{S}$, $\underline{F}$ and $\underline{E}$ [49], the problem can be transformed into a 1D problem. Therefore, it will be assumed from now on that $\underline{S}$, $\underline{F}$ and $\underline{E}$ are vectors. In most practical applications, $\underline{F}$ is constrained to non-negative entries, a physical constraint denoted by $\underline{F} \geqslant \underline{0}$. The inversion problem is then formulated as: *Given $\underline{S}$ and $\underline{K}$, how can $\underline{F}$ be estimated?*

The NNLS algorithm solves the following minimization problem:

$$\underline{F} = \arg\min_{\underline{F}\geqslant\underline{0}} ||\underline{K}\,\underline{F} - \underline{S}||_2^2 \tag{2}$$

where the term being minimized is the called the fidelity term. The fidelity term is an example of a Euclidean or L_2 norm. In general, the L_p norm of a vector $\underline{A}$, with entries a_1, a_2, ..., a_n is defined as:

$$L_p(\underline{A}) = ||\underline{A}||_p = \left(\sum_{i=1}^{n} |a_i|^p\right)^{1/p} \tag{3}$$

If the determinant of the kernel matrix $\underline{K}$ is close to zero (as it is when the transform relating the signal and distributions is composed of exponential decays), the kernel matrix is called ill-conditioned and slight variations in the acquired signal, $\underline{S}$, can lead to significantly different reconstructed distributions, $\underline{F}$. Therefore, the reconstructed distribution from the NNLS algorithm in Eq. (2) is unstable and it does not address the ill-conditioning issue.

Tikhonov regularization addresses the ill–conditioning by looking for a trade–off between the fidelity term and a penalty term which penalizes solutions that do not fit certain constraints:

$$\underline{F} = \arg\min_{\underline{F}\geqslant\underline{0}}\left(\frac{\alpha}{2}||\underline{K}\,\underline{F}-\underline{S}||_2^2+\frac{1}{2}||\underline{R}\,\underline{F}||_2^2\right) \tag{4}$$

where $\underline{R}$ is a regularization matrix and α is a regularization parameter. In the literature, α is sometimes placed in front of the first term and sometimes in front of the second term. In this work, the notation in Eq. (4) will be used. The reason why Tikhonov regularization is more stable than the NNLS algorithm with respect to noise can be explained using a singular value decomposition (SVD) approach [50]. In most occasions, the constraint that one imposes on a physical basis, is for $\underline{F}$ to be smooth. Hence, the preferred $\underline{R}$ would ideally be the matrix that performs the second derivative of $\underline{F}$. While this second derivative operator is easy to construct for 1D matrices, taking the second derivatives of 2D matrices is not straightforward. Therefore this is almost never done. Instead, $\underline{R} = \underline{I}$ (identity matrix), has been exclusively used for the Tikhonov regularization of 2D problems. A small regularization parameter, α, gives a smooth distribution. A large regularization parameter gives a distribution which fits the experimental data better. The main disadvantage of Tikhonov regularization is that it relies on the fact that the distribution $\underline{F}$ is smooth. If the distribution $\underline{F}$ is discrete, i.e. composed of only a few non-zero entries and these features are close to each other, Tikhonov regularization cannot distinguish between these features because it over–smooths the distribution. Therefore, Tikhonov regularization is not suitable for these cases.

2.2. Proposed inversion algorithm

The motivation for the present work is to develop an inversion algorithm which can distinguish close features in sparse distributions, while being stable to high levels of noise. In order to obtain a sparse distribution, $\underline{F}$, it is proposed to solve the following minimization problem:

$$\underline{F} = \arg\min_{\underline{F}\geqslant\underline{0}}\left(\frac{\alpha}{2}||\underline{K}\,\underline{F}-\underline{S}||_2^2+||\underline{F}||_1\right) \tag{5}$$

This will be called an L_1 regularized problem because the penalty term is the L_1 norm of the distribution. The fact that Eq. (5) is regularized will give more stability to noise [35], as compared to the NNLS algorithm. In addition, the use of the L_1 penalty term is expected to give a much sparser solution than the use of the L_2 penalty term in Tikhonov regularization [51].

Eq. (5) is challenging to solve because of the non–differentiability of the L_1 norm. A common technique is to transform Eq. (5) into a primal–dual problem by introducing a dual variable $\underline{Y}$:

$$(\underline{F},\underline{Y}) = \arg\min_{\underline{F}\geqslant\underline{0}}\max_{\underline{Y}}\left(\frac{\alpha}{2}||\underline{K}\,\underline{F}-\underline{S}||_2^2+\underline{Y}^{\mathrm{T}}\underline{F}-\chi(\underline{Y})\right) \tag{6}$$

where $\chi(\underline{Y})$ is an indicator function [52], defined as:

$$\chi(\underline{Y}) = \begin{cases} 0 & ||\underline{Y}||_\infty \leqslant 1 \\ +\infty & ||\underline{Y}||_\infty > 1 \end{cases} \tag{7}$$

Eq. (6) is of the form:

$$(\underline{F},\underline{Y}) = \arg\min_{\underline{F}\geqslant\underline{0}}\max_{\underline{Y}}(g_1(\underline{F})+\underline{Y}^{\mathrm{T}}\underline{F}-g_2(\underline{Y})) \tag{8}$$

with $g_1(\underline{F}) = \alpha/2||\underline{K}\,\underline{F}-\underline{S}||_2^2$ and $g_2(\underline{Y}) = \chi(\underline{Y})$ being convex functions. Eq. (8) can be solved by the Primal-Dual Hybrid Gradient Method (PDHGM) [53]. In overview, the method proposes the following explicit iteration scheme:

$$\begin{cases} \underline{F}^{(k+1)} = (\underline{I}+\tau\partial g_1)^{-1}(\underline{F}^{(k)}-\tau\underline{Y}^{(k)}) \\ \underline{Y}^{(k+1)} = (\underline{I}+\tau\partial g_2)^{-1}(\underline{Y}^{(k)}+\sigma(2\underline{F}^{(k+1)}-\underline{F}^{(k)})) \end{cases} \tag{9}$$

where ∂g_1 denotes the sub-differential of g_1, which is a generalization of the classical differential for convex functions. $(\underline{I}+\tau\,\partial g_1)^{-1}$ is called a resolvent operator, which when applied to a vector $\underline{A}$, is defined as:

$$(\underline{I}+\tau\partial g_1)^{-1}(\underline{A}) = \arg\min_{\underline{X}}\left(\frac{1}{2}||\underline{X}-\underline{A}||_2^2+\tau g_1(\underline{X})\right) \tag{10}$$

The parameters τ and σ are step size parameters, which control convergence and stability of the algorithm. Table 1 describes a pseudocode which implements the iteration scheme in Eq. (9). The iteration scheme will be used in this paper to obtain distributions from L_1 regularized problems.

2.3. Inverse problems in 2D NMR correlation experiments

In this manuscript, we will focus on a particular class of inverse problems, T_1–T_2 and D–T_2 correlation experiments in NMR. It can be shown that the acquired signal in a T_1–T_2 experiment can be expressed as:

$$S(t_1,t_2) = \int_0^\infty\int_0^\infty f(T_1,T_2)(1-2e^{-2t_1/T_1})e^{-t_2/T_2}dT_1dT_2 + E(t_1,t_2) \tag{11}$$

and the acquired signal in a D–T_2 experiment can be expressed as:

$$S(b,t_2) = \int_0^\infty\int_0^\infty f(D,T_2)e^{-bD}e^{-t_2/T_2}dDdT_2 + E(b,t_2) \tag{12}$$

In Eqs. (11) and (12), f is the 2D distribution map, E is the error map, while t_1, t_2 and b are points in the grids of the different dimensions (T_1, T_2 and D) at which signal is acquired. In a discrete version, both equations can be written as:

$$\underline{S} = \underline{K}\,\underline{F} + \underline{E} \tag{13}$$

Table 1
Pseudocode that solves Eq. (9) numerically, based on the PDHGM method.

Step 1. Choose algorithm step parameters τ, σ and the regularization parameter, α
Step 2. Set the convergence tolerance, *TOL*
Step 3. Calculate $\underline{B} = (\underline{I}+\tau\alpha\underline{K}^{\mathrm{T}}\underline{K})^{-1}$
Step 4. Initialize $\underline{Y}^{(0)} = \underline{0}, \underline{F}^{(0)} \neq \underline{0}$ and $\tilde{\underline{F}}^{(0)} = \underline{F}^{(0)}$
Step 5. Initialize count number, $k = 1$ and convergence tracker, $\epsilon^{(0)} = 1$
Step 6. **while** $\epsilon^{(k)} > TOL$ **do**
a. $\tilde{\underline{Y}}^{(k)} \leftarrow \underline{Y}^{(k-1)} + \sigma\tilde{\underline{F}}^{(k-1)}$
b. $\underline{Y}^{(k)} \leftarrow \frac{\tilde{\underline{Y}}^{(k)}}{\max(1,|\tilde{\underline{Y}}^{(k)}|)}$ All operations in this line are element-wise.
c. $\underline{F}^{(k)} \leftarrow \underline{B}(\tilde{\underline{F}}^{(k-1)} - \tau\underline{Y}^{(k)} + \tau\alpha\underline{K}^{\mathrm{T}}\underline{S})$
d. $\underline{F}^{(k)} \leftarrow \max(0,\underline{F}^{(k)})$ All operations in this line are element-wise
e. $\tilde{\underline{F}}^{(k)} \leftarrow 2\underline{F}^{(k)} - \underline{F}^{(k-1)}$
f. $\epsilon^{(k)} \leftarrow \frac{||\underline{F}^{(k)}-\underline{F}^{(k-1)}||_2}{||\underline{F}^{(k-1)}||_2}$
g. $k \leftarrow k+1$
end while

Therefore, T_1–T_2 and D–T_2 experiments can be treated as inverse problems.

3. Experimental

3.1. Materials

NMR measurements were conducted on a number of liquid samples in bulk and imbibed within a porous medium. Liquids used were: water deionised using PURELAB®; n–hexane (Sigma Aldrich, ≥99.7% purity); and n–dodecane (Sigma Aldrich, ≥99.8% purity). The porous medium used was meso-porous silica beads of approximately spherical shape and diameter of 3–4 mm and with a mean pore size of 10 nm, provided by Johnson Matthey. Gadolinium (III) chloride hexahydrate ($GdCl_3{\cdot}6H_2O$) (Alfa Aesar, ≥99.8% REO purity) was used to reduce the relaxation time constant of water. Electronic scales (Precisa 205 A) with a precision of 0.1 mg were used for gravimetric measurements. Validation of the NMR concentration measurements was made by Gas Chromatography (GC) (Agilent Technologies 7890A). The calibration standard error on the GC concentration measurements was 20 ng μl^{-1} on a 1 μl sample.

Four pairs of samples were prepared for testing the proposed inversion technique. These correspond to samples in which separation of the NMR signals is of increasing difficulty.

(i) Two solutions of $GdCl_3{\cdot}6H_2O$ in water were prepared which had concentrations of 0.25 mM and 0.36 mM. From these solutions, two samples were prepared: sample A1 was simply the 0.25 mM solution; sample A2 was composed of the two solutions which were physically separated with a volume ratio 1:1.
(ii) Two samples composed of bulk binary liquid mixtures of hexane and dodecane were prepared, with respective mass fractions of dodecane of 0.267 ± 0.003 (sample B1) and 0.532 ± 0.003 (sample B2).
(iii) Two samples composed of binary mixtures of hexane and dodecane imbibed within silica beads were prepared as follows: A binary bulk mixture of known mass fraction was initially prepared and the silica beads were immersed in the mixture. After 24 h, the beads were taken out and the draining liquid removed. The composition of the liquid imbibed within the beads was calculated by measuring the composition of the remaining bulk liquid using GC and performing a mass balance. The dodecane mass fractions of the liquid imbibed within the beads were calculated to be 0.20 ± 0.02 (sample C1) and 0.45 ± 0.05 (sample C2), respectively.
(iv) Two samples composed of mixtures of hexane and dodecane residing both inside the silica beads (intra particle) and between the silica beads (inter particle) were prepared by immersing the silica beads into each of two bulk binary mixtures of hexane and dodecane; the two bulk liquid mixtures being characterised by dodecane mass fractions of 0.246 ± 0.003 (sample D1) and 0.516 ± 0.003 (sample D2), respectively. The NMR measurements were then performed on the immersed beads.

3.2. NMR acquisitions

All experiments were conducted on a Bruker DMX300 spectrometer, operating at a resonant frequency of 300.13 MHz for ^1H observation. The maximum gradient amplitude of the gradient set was 1176 G cm^{-1} and the radiofrequency (RF) coil had a diameter of 5 mm. Experiments were performed at a temperature of 20 ± 1 °C.

1D NMR relaxation time analysis and diffusion experiments were performed on the individual chemicals used and for pure single-component hexane and decane imbibed within the silica beads, as follows. The Carr-Purcell-Meiboom-Gill (CPMG) [54,55] or PROJECT [56] pulse sequences were used to measure T_2; the Inversion-Recovery (IR) [57] pulse sequence was used to measure T_1; the Pulsed Field Gradient Stimulated Echo (PGSTE) [58] pulse sequence was used to measure D. The PROJECT sequence was used for the experiments where the samples contained hexane or dodecane in order to suppress J–modulation. The results from these 1D experiments are summarized in Table 2; these are used as reference values for the 2D NMR correlation experiments.

The pulse sequence used for the T_1–T_2 correlation experiments of the water solutions was an IR–CPMG [24] sequence. The pulse program used for the D–T_2 correlation experiments of the water solutions was a PGSTE–CPMG [11] sequence. For the mixtures of hexane and dodecane, the CPMG sequence was substituted with a PROJECT sequence.

The echo time in the CPMG and PROJECT sequences was 1 ms and the maximum number of echoes was such that the maximum time observed in the T_2 decay was $\sim 5T_2$. For the IR pulse sequence, the maximum time observed in the T_1 decay was $\sim 5T_1$. The diffusion time in the PGSTE sequence was 5 ms, the gradient pulse duration was 1 ms and the maximum gradient strength was such that an attenuation of the signal to ~0.5% of the maximum value was achieved in the Stejskal-Tanner decay. The number of data points used for the IR and PGSTE sequences was 16, apart from the experiment to characterise liquid mixtures present in both the inter and intra particle space (i.e., samples D1 and D2), in which case 32 steps were used.

The data points for the IR, PGSTE, CPMG and PROJECT sequences were spaced linearly for all experiments, apart from the experiments on samples D1 and D2. In the case of samples D1 and D2, four components are expected in the distribution maps. In these systems, we expect the two intra particle relaxation time constants and diffusion coefficients to be similar to each other, but relatively different to the two inter particle values. In turn, we expect the two inter particle measurements of the relaxation time constants and diffusion coefficients to be similar. For this case, the linear sampling scheme did not offer enough resolution. In particular, in the case in which we wish to identify 4 diffusion coefficients where $D_1 > D_2 \gg D_3 > D_4$, the linear sampling scheme will resolve the two pairs (D_1, D_2) and (D_3, D_4) but does not resolve within the pairs (i.e. D_1 from D_2, or D_3 from D_4). In order to get a better resolution, the sampling density of points, $\rho(b)$, was changed from linear to being proportional to the following expression:

Table 2
The relaxation time constants, T_1, T_2 and diffusion coefficient, D, of the chemicals used in the experiments, obtained using 1D NMR relaxation and diffusion experiments. The quoted uncertainty is the fitting standard error.

Material	T_1/s	T_2/s	D ($\times 10^{-9}$)/ $m^2\ s^{-1}$
0.25 mM $GdCl_3{\cdot}6H_2O$ solution	0.150 ± 0.005[a]	0.120 ± 0.004[b]	2.00 ± 0.03[d]
0.36 mM $GdCl_3{\cdot}6H_2O$ solution	0.080 ± 0.004[a]	0.080 ± 0.003[b]	2.00 ± 0.04[d]
Pure bulk hexane	1.90 ± 0.01[a]	1.60 ± 0.01[c]	3.80 ± 0.05[d]
Pure bulk dodecane	1.00 ± 0.02[a]	0.88 ± 0.03[c]	0.76 ± 0.02[d]
Pure hexane imbibed in silica beads	1.30 ± 0.06[a]	0.60 ± 0.05[c]	2.50 ± 0.06[d]
Pure dodecane imbibed in silica beads	0.74 ± 0.03[a]	0.48 ± 0.02[c]	0.43 ± 0.02[d]

[a] Obtained from IR pulse sequence.
[b] Obtained from CPMG pulse sequence.
[c] Obtained from PROJECT pulse sequence.
[d] Obtained from PGSTE pulse sequence.

$$\rho(b) \propto (e^{-bD_4} - e^{-bD_3}) + (e^{-bD_2} - e^{-bD_1}) \tag{14}$$

with b being defined in Eq. (12). This sampling scheme effectively allows denser sampling in the regions where there is a larger difference between the signals acquired from components of similar diffusion coefficients.

3.3. Implementation of the algorithm

The 2D time-domain NMR signals were initially projected onto a truncated singular value basis of the kernel matrix [59]. All distribution maps were reconstructed on a 32×32 grid, with linearly spaced points. This makes the quantification of the amounts of each component straightforward. Simulations showed that the relative performance of the NNLS method, Tikhonov and L_1 regularization with linearly spaced points in the distribution maps is similar to the case when logarithmically spaced points are used, which is also commonly performed in the literature.

The regularization parameter, α, for Tikhonov regularization was chosen using the Generalized Cross Validation (GCV) method [60]. In GCV, for a given α, each point in the NMR signal is removed in turn (cross-one out method) and the distribution reconstructed. The difference between the actual removed point and the predicted value of that point from the reconstructed distribution is noted. An average of all these values is called the GCV score for that value of α:

$$\mathrm{GCV}(\alpha) = \frac{s||\underline{K}\,\underline{F} - \underline{S}||_2^2}{(s - m(\alpha))^2} \tag{15}$$

where:

$$m(\alpha) = \mathrm{tr}(\alpha\underline{K}(\alpha\underline{K}^T\underline{K} + \underline{I})^{-1}\underline{K}^T) \tag{16}$$

is known as the effective number of parameters or the degrees of freedom for Tikhonov regularization and s is the size of $\underline{S}$. The best value for α is then chosen at the minimum of this curve.

The regularization parameter, α, in the L_1 regularization problem was chosen using a variant of GCV. An analytical expression for the GCV curve does not exist in this case. However, by rewriting Eq. (5) as:

$$\underline{F} = \arg\min_{\underline{F}\geq\underline{0}}\left(\frac{\alpha}{2}||\underline{K}\,\underline{F} - \underline{S}||_2^2 + \sum_{i=1}^{n}\frac{F_i^2}{|F_i|}\right) \tag{17}$$

(where n is the size of $\underline{F}$) which looks similar to Tikhonov regularization, one can approximate the degrees of freedom of an L_1 regularization problem by [61,62]:

$$m(\alpha) = \mathrm{tr}(\alpha\underline{K}(\alpha\underline{K}^T\underline{K} + \underline{W}^-)^{-1}\underline{K}^T) \tag{18}$$

where $\underline{W}^-$ is the generalized inverse of $\underline{W}$, with $\underline{W}$ defined as $\mathrm{diag}(|F_i|)$. This value of the degrees of freedom can then be used to calculate the GCV score in Eq. (15). The best value of α is again found at the minimum of the score. More accurate estimations of the degrees of freedom in the L_1 regularization problem have been recently devised [63–65]. However, they are less practical to calculate and were not used in this work.

From a statistical point of view, GCV is a model selection method, similar to the Akaike Information Criterion (AIC) [66], Bayesian Information Criterion (BIC) [67] or C_p method [68], in the sense that it invokes a parsimony argument: as the regularization parameter α changes, the number of fitted parameters $m(\alpha)$ varies, and model selection methods decide on the optimal α based on a trade–off between fidelity to the data and $m(\alpha)$. Although GCV has been the most commonly used model selection method, other methods have also been used in the inversion of 2D NMR correlation data [21]. Practically, all these methods give very similar results, but GCV is more practical as it does not require a knowledge of the noise level in the data.

Other methods of choosing the regularization parameter for the L_1 regularization problem were also considered: in particular, the adaptation of the L–curve method [69] in Tikhonov regularization to the L_1 regularization problem (called the Pareto curve [70]) and the Morozov discrepancy principle [71]. However, simulations showed that the Pareto curve is unsuitable for T_1-T_2 and D-T_2 experiments because $||\underline{F}||_1$ is constrained by the first signal point acquired, $S(0)$, while the Morozov discrepancy principle was sensitive to the estimate of the noise level in the acquired signal. Therefore, these two methods were not used in choosing the regularization parameter.

The uncertainty in the magnitude of each peak in the distribution map is estimated using an adaptation of the Cramér–Rao Lower Bound (CRLB) theory [72]. In overview, the CRLB theory states that the variance of the parameters F_i which we are trying to extract has a lower bound, related to the Fisher Information Matrix $\underline{M}(\underline{F})$ by the inequality:

$$\mathrm{Var}(F_i) \geqslant (\underline{M}^{-1}(\underline{F}))_{ii}. \tag{19}$$

Assuming Gaussian noise of variance σ^2 in Eq. (1), the Fisher Information Matrix simplifies to $\underline{M}(\underline{F}) = 1/\sigma^2\ \underline{K}^T\underline{K}$, which is not a function of $\underline{F}$. However, since $\underline{K}$ is ill-conditioned, estimating the inverse of $\underline{M}$ is unstable. Therefore, it is impractical to assign error estimates for all the elements of $\underline{F}$. However, it is possible to assign error estimates on the non-zero elements of $\underline{F}$ (the peaks of the distribution) using the method that follows. If it is assumed that the map has k discrete peaks whose indices are in a set Ω (such that if $i \in \Omega$, $F_i > 0$ and if $i \notin \Omega$, $F_i = 0$), then $\underline{M}(\underline{F}) = 1/\sigma^2\ \underline{K}_\Omega^T\underline{K}_\Omega$, where $\underline{K}_\Omega$ is the kernel matrix $\underline{K}$ with only the columns whose indices are in Ω. The estimated uncertainties using this approach, termed the oracle estimates [73], are low because of the assumption of having prior knowledge of the position of the peaks. In order to correct for this assumption, it has been proved [74–76] that the true estimate of the variance of any of the parameters is related to the oracle estimate with a high probability by only a constant factor:

$$\mathrm{Var}(F_i) = ck\ln(n)\sigma^2((\underline{K}_\Omega^T\underline{K}_\Omega)^{-1})_{ii} \tag{20}$$

where c is a constant which depends on the application and the normalization of the signal. For the T_1–T_2 and D–T_2 correlation experiments with the NMR signal being normalized to a maximum of 1, simulations showed that $c = 0.25$ gives reliable estimates for the uncertainties.

The method described above for estimating the uncertainties in the magnitude of the peaks of the distribution is not specific to the algorithm introduced in this work; it can also be applied if other algorithms are used to solve the L_1 regularization problem. Apart from being able to assign error estimates, the method can be used to determine *a priori* whether L_1 regularization is capable of quantifying the different peaks, therefore guiding experimental design. Indeed, if prior knowledge exists of where to expect the peaks in the distribution maps, one can calculate the uncertainties expected using Eq. (20) and arrive at a decision on whether those uncertainties are low enough for the L_1 regularization to be used or not. Further, given that the kernel matrix $\underline{K}$ depends on the sampling pattern (the particular values of t_1, t_2 and b in Eq. (11) and Eq. (12)), Eq. (20) can be used to customize the sampling pattern in order to achieve a desired uncertainty level.

The convergence of the algorithm in Table 1 is guaranteed if the following condition is met [53]:

$$\tau\sigma \leqslant 1 \tag{21}$$

However, the particular choice of τ and σ is heuristic. A smaller τ will increase the stability while reducing the convergence speed of the algorithm. A good compromise between the two was found

when $\tau = 0.1$ and $\sigma = 10$. The best values of τ and σ will depend slightly on the scaling of the signal. To avoid this, it is best to normalize the NMR signal to a maximum of 1, a technique which was followed in this study.

The algorithmic complexity of the algorithm is $O(n)$. A typical number of iterations needed for the algorithm to converge was 10,000. The time in which this convergence is achieved for a 32×32 distribution map will depend on the processing speed of the computer. With a 2.0 GHz CPU and 16 GB RAM, 10,000 iterations took approximately 17 s.

The initialization of the algorithm has no impact on the reconstructed distribution because the function being minimized is convex. Practically, it was also observed that the convergence speed is unaffected.

4. Results and discussion

Initially, experimental results on a single component sample are used to investigate the stability to noise of the L_1 regularization method, as compared to the NNLS and Tikhonov regularization methods. Then, experimental results of bulk binary liquid mixtures and binary liquid mixtures imbibed within the porous beads systems are used to compare the spectral resolution of the L_1 regularization method and the Tikhonov regularization method. Finally, the L_1 regularization method is used to process 2D NMR correlation experiments of mixtures of hexane and dodecane in different physical environments (i.e., inter and intra particle space) where the NNLS and Tikhonov regularization methods fail to distinguish between the different components.

4.1. Stability to noise

To test the stability of algorithms to noise, experiments were performed on a single component sample and increasing levels of Gaussian noise were added. T_1–T_2 and D–T_2 experiments were performed on sample A1, the 0.25 mM $GdCl_3{\cdot}6H_2O$ solution. From Table 2, the distributions are expected to have one peak at $T_1 = 0.150 \pm 0.005$ s, $T_2 = 0.120 \pm 0.004$ s and $D = (2.00 \pm 0.03) \times 10^{-9}$ m^2 s^{-1}. Random Gaussian noise of increasing magnitude was added to the 2D NMR signal, such that a range of signal to noise ratios (SNR) from 5000 to 5 was studied. The 2D distributions were then reconstructed by applying the NNLS and the L_1 regularization method. For SNR > 20, no difference was seen in the reconstructions from the NNLS algorithm and the L_1 regularization method. For this reason, they are not shown here. However, for SNR < 20, the NNLS method failed to reconstruct the distribution accurately, incorrectly predicting more than one peak in the distribution. In contrast, the L_1 minimization method correctly predicted the distributions at all SNR studied.

Fig. 1 shows the reconstructed T_1–T_2 and D–T_2 distributions from the NNLS and L_1 regularization methods at SNR = 20. The NNLS algorithm incorrectly predicts two peaks in both T_1–T_2 and D–T_2 maps, while the L_1 regularized problem predicts the position of the single peak in the distribution at $T_1 = 0.15 \pm 0.01$ s, $T_2 = 0.12 \pm 0.01$ s and $D = (2.0 \pm 0.1) \times 10^{-9}$ m^2 s^{-1}, which is in excellent agreement with the expected values shown in Table 2.

Over the full range of SNR studied, no difference was observed between the reconstructed distributions from the L_1 and Tikhonov regularization methods and both methods reconstructed the distributions accurately. Therefore, the reconstructions from Tikhonov regularization are not shown.

The stability to noise offered by the L_1 regularization method can be used to reduce the extent of signal averaging that is needed to achieve sufficient SNR for subsequent analysis. Since SNR is proportional to $B_0^{7/4}$, where B_0 is the permanent magnetic field strength [77], this method could therefore be useful in extending measurement capabilities at low magnetic field.

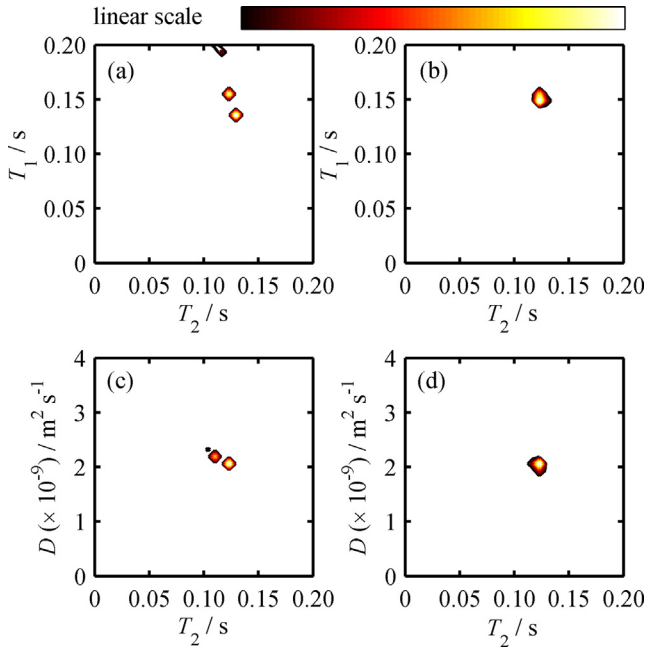

Fig. 1. (a, b) T_1–T_2 and (c, d) D–T_2 distribution maps of sample A1, a 0.25 mM $GdCl_3{\cdot}6H_2O$ deionised water solution, reconstructed for SNR = 20 using (a, c) the NNLS and (b, d) L_1 regularization methods.

4.2. Spectral resolution

In order to compare the spectral resolution of algorithms, experiments were performed on a two-component sample, in which the resolution of the signal from the individual components is expected to be challenging using Tikhonov regularization. T_1–T_2 and D–T_2 experiments were performed on sample A2, composed of two physically separate $GdCl_3{\cdot}6H_2O$ solutions of concentrations 0.25 and 0.36 mM and volume ratio 1:1. From Table 2, it is expected that the distribution maps will show two peaks: one at $T_1 = 0.150 \pm 0.005$ s, $T_2 = 0.120 \pm 0.004$ s and $D = (2.00 \pm 0.03) \times 10^{-9}$ m^2 s^{-1} and the other at $T_1 = 0.080 \pm 0.004$ s, $T_2 = 0.080 \pm 0.003$ s and $D = (2.00 \pm 0.04) \times 10^{-9}$ m^2 s^{-1}.

Fig. 2 shows the reconstructed T_1–T_2 and D–T_2 distribution maps obtained using Tikhonov and L_1 regularization methods. It can be seen that Tikhonov regularization cannot distinguish between the two solutions; the peaks associated with each of the two solutions are included in a single broad peak. This is to be expected since the resolution of Tikhonov regularization is typically limited to a factor of 3 in the relaxation times or diffusion coefficients [6]. In contrast, the L_1 regularization method predicts two peaks: one at $T_1 = 0.15 \pm 0.01$ s, $T_2 = 0.12 \pm 0.01$ s and $D = (2.0 \pm 0.1) \times 10^{-9}$ m^2 s^{-1}, corresponding to the 0.25 mM solution, and the other at $T_1 = 0.08 \pm 0.01$ s, $T_2 = 0.08 \pm 0.01$ s and $D = (2.0 \pm 0.1) \times 10^{-9}$ m^2 s^{-1}, corresponding to the 0.36 mM solution. The position of these peaks is in excellent agreement with those given in Table 2 for each of the component liquids. In addition, the ratio of the amounts of each solution present, measured by the ratio of the areas of each peak in the maps is 1.0 (to 2 s. f.), for both T_1–T_2 and D–T_2 distribution maps, consistent with the 1:1 volume ratio of the two-component sample.

The SNR in the acquired T_1–T_2 and D–T_2 signals was 3000 and 1900, respectively. At these high SNR, no difference was observed between the reconstructed maps by the L_1 regularization and NNLS

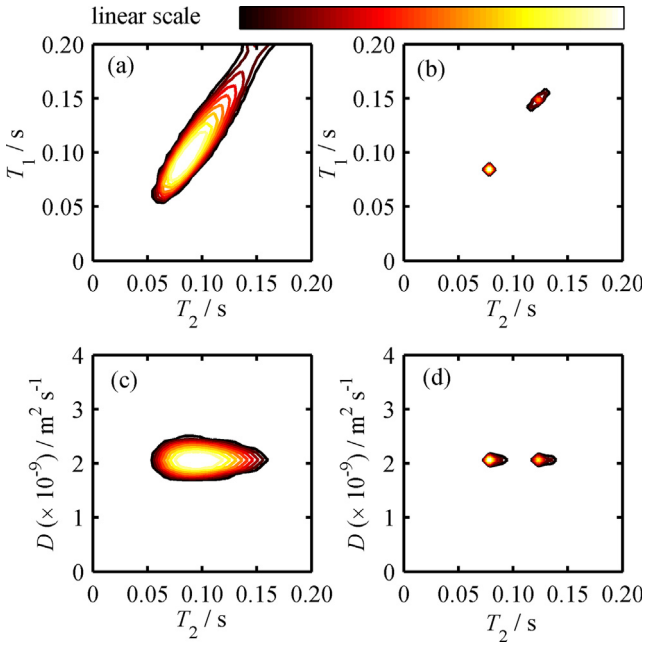

Fig. 2. (a, b) T_1–T_2 and (c, d) D–T_2 distribution maps of sample A2, composed of physically separate 0.25 and 0.36 mM $GdCl_3{\cdot}6H_2O$ deionised water solutions, reconstructed using (a, c) Tikhonov regularization and (b, d) L_1 regularization methods. The SNR in the NMR signal was 3000 for the T_1–T_2 experiment and 1900 for the D–T_2 experiment. The component with the larger T_2 is the 0.25 mM solution.

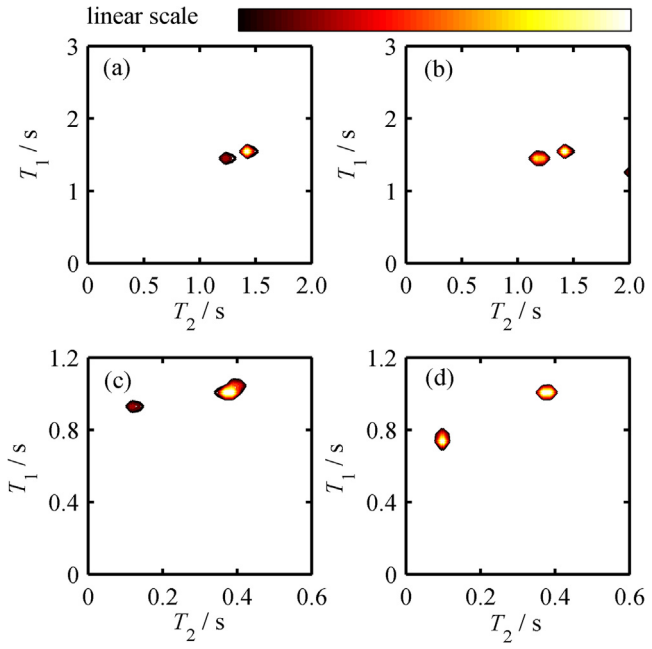

Fig. 3. T_1–T_2 distribution maps of mixtures of hexane and dodecane (a, b) in bulk and (c, d) imbibed within silica beads, reconstructed using the L_1 regularization method. The samples shown are (a) sample B1, (b) sample B2, (c) sample C1, and (d) sample C2. The component with the larger T_2 is hexane. The SNR in the NMR signal was approximately 2500 in all the experiments.

methods. Therefore, the reconstructed maps from the NNLS method are not shown.

These results show that the L_1 regularization method has the potential to be used to resolve features in inverse problems which were previously unable to be resolved by methods such as Tikhonov regularization. This conclusion is in agreement with the observations of Benjamini and Basser [37].

4.3. Resolving individual components of mixtures: Hexane and dodecane in bulk liquid mixtures and within porous media

In this section we apply the inversion algorithms to samples for which both NNLS and Tikhonov regularization fail to predict the distributions, while the L_1 regularization method succeeds. T_1–T_2 and D–T_2 experiments were performed on bulk liquid mixtures of hexane and dodecane (samples B1 and B2) and mixtures of hexane and dodecane imbibed within silica beads (samples C1 and C2). Samples at different mass fractions of dodecane are included to demonstrate the quantitative nature of the method at different concentrations. It is well known that the relaxation time constants and diffusion coefficients of alkanes in a mixture become more similar relative to the pure single component values [78,79]; the relaxation time constants and diffusion coefficient of an alkane in a mixture depend not only on the chain length of the alkane, but also on the mean chain length of the mixture. Therefore, we would expect that in the T_1–T_2 and D–T_2 maps the peaks corresponding to hexane and dodecane would be closer to one another than the values in Table 2 suggest, making it more difficult to resolve these chemicals.

Fig. 3 shows the T_1–T_2 distribution maps of the bulk mixtures of hexane and dodecane and of the mixtures of hexane and dodecane imbibed within silica beads, reconstructed using the L_1 regularization method. Figs. 3(a) and 3(b) show the T_1–T_2 distribution maps of two different bulk mixtures, with corresponding dodecane mass fraction of 0.267 ± 0.003 (sample B1) and 0.532 ± 0.003 (sample B2). Two peaks are clearly observable in both distribution maps: hexane at $T_1 = 1.5 \pm 0.1$ s, $T_2 = 1.4 \pm 0.1$ s and dodecane at $T_1 = 1.4 \pm 0.1$ s, $T_2 = 1.2 \pm 0.1$ s. Fig. 3(c) and (d) show the T_1–T_2 distribution maps of two different mixtures of hexane and dodecane imbibed within silica beads, with corresponding dodecane mass fractions of 0.20 ± 0.02 (sample C1) and 0.45 ± 0.05 (sample C2). Two peaks are clearly identified in these maps: intra particle hexane at $T_1 = 1.0 \pm 0.1$ s, $T_2 = 0.4 \pm 0.04$ s and intra particle dodecane at $T_2 = 0.10 \pm 0.02$ s. The relaxation constant T_1 of intra particle dodecane is $T_1 = 0.94 \pm 0.04$ s for sample C1 and $T_1 = 0.78 \pm 0.04$ s for sample C2. The relaxation time constants T_2 of the intra particle liquid are significantly shorter than the corresponding values in the bulk liquid mixture due to the additional dephasing of nuclear spins caused by the magnetic heterogeneity in the porous medium and the interaction with the pore surface [9].

Fig. 4 shows the corresponding D–T_2 distribution maps for the same samples discussed in Fig. 3; the D–T_2 distribution maps have been reconstructed using the L_1 regularization method. Fig. 4 (a) and (b) show the D–T_2 distribution maps of samples B1 and B2, while Fig. 4(c) and (d) show the D–T_2 distribution maps of samples C1 and C2. Hexane and dodecane are clearly identifiable in all of these maps. The relaxation time constants T_2 obtained using the D–T_2 maps differ by <10% from the corresponding relaxation constants T_2 obtained using the T_1–T_2 maps. The agreement between the T_1–T_2 and D–T_2 data effectively reduces the uncertainty in the measured T_2.

The results in Figs. 3 and 4 show that the L_1 regularization method can resolve components in T_1–T_2 and D–T_2 distribution maps even if their difference in relaxation constants is as low as 10%. This is a major improvement over the factor of 3 that the resolution of Tikhonov regularization is typically limited to [6].

Both the NNLS and Tikhonov regularization methods failed to reconstruct the T_1–T_2 and D–T_2 distributions correctly. One example of this is shown for sample C2 in Fig. 5. Sample C2 is chosen as it represents one of the cases in which, relative to the other samples, it should be easier for the NNLS and Tikhonov regularization

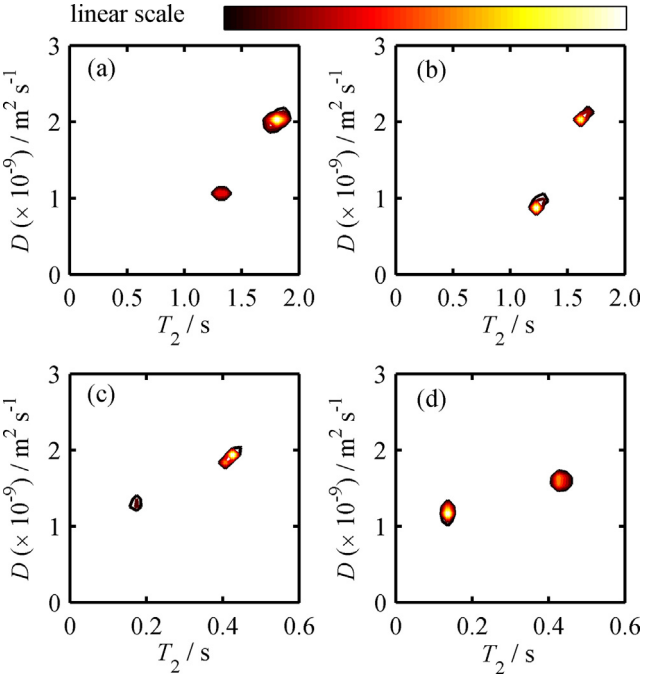

Fig. 4. D–T_2 distribution maps of mixtures of hexane and dodecane (a, b) in bulk and (c, d) imbibed within silica beads, reconstructed using the L_1 regularization method. The samples shown are (a) sample B1, (b) sample B2, (c) sample C1, and (d) sample C2. The component with the larger T_2 is hexane. The SNR in the NMR signal was approximately 2000 in all the experiments.

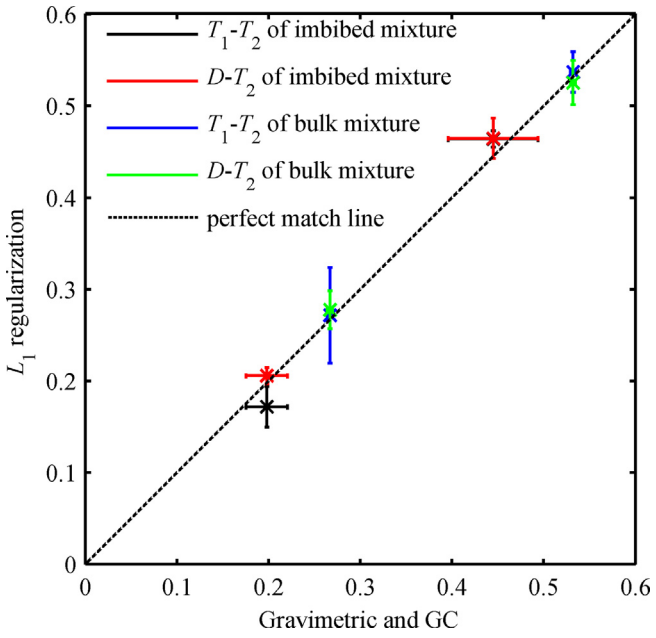

Fig. 6. Comparison of dodecane mass fraction measured using the L_1 regularization method in the inversion of 2D NMR correlation experiments with the mass fraction measured using the gravimetric and GC methods described in Section 3.1. As discussed in the text, larger errors are associated with GC analysis compared to gravimetric measurements.

methods to predict the correct distributions because the components have a difference in the expected T_2 of a factor of 4. Fig. 5 (a) shows the D-T_2 distribution of sample C2, reconstructed using the NNLS method. Three peaks are predicted from the method, when only two are expected. The prediction of extra peaks is a typical artefact of the NNLS method. Fig. 5(b) shows the D–T_2 distribution of sample C2, reconstructed using the Tikhonov regularization method. The method predicts a single broad peak (extending over the range of the two expected peaks). This is a typical artefact of the Tikhonov regularization method.

Quantitative comparison of the mass fraction of dodecane measured from the T_1–T_2 and D–T_2 distribution maps in Figs. 3 and 4 is shown in Fig. 6 with the mass fraction of dodecane measured using gravimetric and GC methods. The first observation is that the mass fractions of dodecane measured using the T_1–T_2 maps has an average difference of 0.02 from the corresponding mass fractions of dodecane measured using the D–T_2 maps. The second observation is that each of these measures has an average difference of 0.01 from the measurements using gravimetric and GC methods. The results in Fig. 6 therefore show that, in addition to being able to resolve very close features, the L_1 regularization method can be used quantitatively to obtain information on the amounts of each component present, even when the liquid mixture is imbibed within the porous medium.

4.4. Resolving inter and intra particle hexane and dodecane compositions

In this section, the L_1 regularization method is applied to determine D, T_2 and the chemical composition of hexane and dodecane mixtures imbibed within porous silica beads which remain

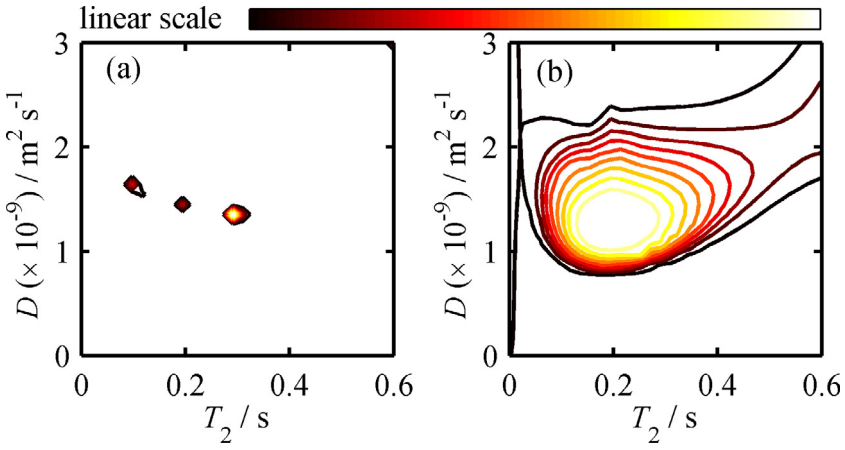

Fig. 5. D–T_2 distribution maps of sample C2, a mixture of hexane and dodecane imbibed within silica beads, reconstructed using (a) the NNLS and (b) Tikhonov regularization methods. The SNR in the NMR signal was 2000.

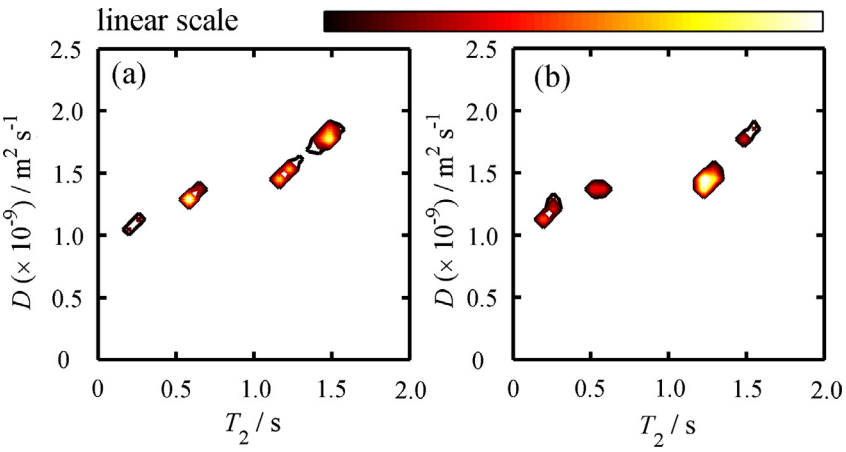

Fig. 7. D–T_2 distribution maps of (a) sample D1 and (b) sample D2, which are liquid mixtures of hexane and dodecane in silica beads with inter and intra particle liquid present. In an order of increasing T_2, the peaks correspond to intra particle dodecane, intra particle hexane, inter particle dodecane and inter particle hexane. The SNR in the NMR signal was approximately 1500 in both experiments.

Table 3
The relaxation time constants, T_2, and the diffusion coefficients, D, of the components in samples D1 and D2, extracted from a D–T_2 correlation experiment processed with the L_1 regularization method. The D-T_2 maps are shown in Fig. 7.

Component	Sample D1		Sample D2	
	T_2/s	D ($\times 10^{-9}$)/m^2 s^{-1}	T_2/s	D ($\times 10^{-9}$)/m^2 s^{-1}
Inter particle hexane	1.4 ± 0.1	1.7 ± 0.2	1.5 ± 0.1	1.8 ± 0.1
Inter particle dodecane	1.2 ± 0.1	1.5 ± 0.1	1.3 ± 0.1	1.5 ± 0.1
Intra particle hexane	0.6 ± 0.1	1.3 ± 0.1	0.6 ± 1	1.4 ± 0.1
Intra particle dodecane	0.2 ± 0.1	1.1 ± 0.1	0.2 ± 0.1	1.2 ± 0.1

immersed in the bulk liquid mixture. D–T_2 experiments were performed on samples D1 and D2. Four peaks are expected in the D–T_2 distribution maps, corresponding to intra particle dodecane, intra particle hexane, inter particle dodecane and inter particle hexane.

Fig. 7 shows the D–T_2 distribution maps of samples D1 and D2 reconstructed using the L_1 regularization method. Four components are clearly observable in each of the maps. The values of the relaxation time constant, T_2, and the diffusion coefficient, D, extracted from these distributions for each of the components is given in Table 3. Although there is less than 10% difference in the relaxation time constants and diffusion coefficients of the inter particle or the intra particle components, the L_1 regularization method has successfully resolved them.

The D–T_2 maps were used to estimate the total mass fraction of dodecane in each of the samples. For sample D1 this was estimated to be 0.22 ± 0.04 and for sample D2 this was estimated to be 0.53 ± 0.02. These mass fractions differ by less than 0.03 from the measurements using the gravimetric technique demonstrating that the L_1 regularization method can be used quantitatively.

More importantly, the maps in Fig. 7 can be used to obtain the inter and intra particle composition of the liquid. The dodecane mass fraction for the inter particle liquid in samples D1 and D2 is 0.30 ± 0.02 and 0.59 ± 0.02, respectively. The dodecane mass fraction for the intra particle liquid in samples D1 and D2 is 0.19 ± 0.03 and 0.43 ± 0.02, respectively. The ability to obtain the difference in the concentration between the inter and intra particle liquid is invaluable in, for example, identifying mass transfer limitations in heterogeneous catalysts.

T_1–T_2 experiments were also performed on these samples. However, the L_1 regularization method was unable to resolve between the inter particle hexane and inter particle dodecane. Both the NNLS and Tikhonov regularization methods were unable to reconstruct neither the T_1–T_2 nor the D–T_2 distribution maps. These maps are not shown here.

4.5. Potential and limitations

It was shown in Sections 4.1–4.4 that the proposed L_1 regularization method is able to reconstruct sparse T_1–T_2 and D–T_2 distribution maps, even if the components of the maps differ in relaxation time constants or diffusion coefficients by less than 10% or if the SNR < 20. These are considerable improvements over the capabilities of the NNLS and Tikhonov regularization methods. The L_1 regularization method can be applied in a similar way to other 2D NMR correlation experiments [42–45]. In addition, the method can be applied to other inverse problems in science and engineering [1–5], as long as the distribution is expected to be sparse. The only modification needed is the kernel function, $\underline{K}$, which is specific to a given application.

The algorithm is recommended only for cases in which there is a prior knowledge that the distribution is sparse. If the true distribution is broad, the algorithm can give inaccurate reconstructions. When applying the L_1 regularization method, the typical indication that the true distribution might actually be broad is if the reconstructed distribution shows a cluster of peaks within a narrow region.

5. Conclusions

L_1 regularization has attracted recent attention in processing ill–conditioned sparse inverse problems. A robust algorithm was introduced to numerically solve the L_1 regularized problem and methods were described for objectively choosing the amount of

regularization needed and assigning error estimates to the reconstructed maps. The L_1 regularization method was applied to a class of ill–conditioned inverse problems: spin–lattice relaxation – spin–spin relaxation, T_1–T_2, and diffusion – spin–spin relaxation, D–T_2, correlation experiments in NMR. It was shown that the L_1 regularized problem is stable even at SNR < 20, while the conventional NNLS method fails at these high values of noise. In addition, it was shown that using the L_1 regularization method, components with relaxation time constants and diffusion coefficients differing by as little as ~ 10% can be resolved. The typical resolution limitation of the conventional Tikhonov regularization is a factor of 3 difference in the relaxation time constants and diffusion coefficients. The increased resolution capability obtained from the algorithm presented here was used to extract inter and intra particle liquid compositions of a binary mixture of hexane and dodecane. This measurement capability will be valuable in extending our ability to characterise the composition, and chemically-specific molecular diffusion and surface interaction properties of multi-component mixtures in porous media. Amongst other applications, it offers a method to directly characterise mass transfer limitations in heterogeneous catalysts. Further, the robustness to noise of the method makes it particularly applicable to low field measurements and its ability to separate similar coefficients could be very useful in separating similar molecules in DOSY (diffusion NMR) experiments. The L_1 regularization method can be easily extended to other 2D NMR correlation experiments and ill–conditioned inverse problems from molecular dynamics to tomography. The only prerequisite is that the expected property needs to be sparse.

Acknowledgments

A.R. acknowledges Gates Trust Cambridge for financial support. A.J.S. and L.F.G. would like to acknowledge support from EPSRC (EP/N009304/1). The authors would like to thank Dr Martin Benning for the help in choosing a suitable algorithm, Mohamed Ainte for the help in preparing the samples and Tian Li for the help with sample analysis.

References

[1] D. Jensen, A. Wasserman, Numerical density–to–potential inversions in time–dependent density functional theory, Phys. Chem. Chem. Phys. 18 (2016) 21079.
[2] M.V. Ivanov, M.R. Talipov, Q.K. Timerghazin, Electrostatic point charge fitting as an inverse problem: revealing the underlying ill–conditioning, J. Chem. Phys. 143 (2015) 134102.
[3] E. Elizade, R. Urtega, R.R. Koropecki, C.L.A. Berli, Inverse problem of capillary filling, Phys. Rev. Lett. 112 (2014) 134502.
[4] P. Kügler, E. Gaubitzer, S. Müller, Parameter identification for chemical reaction systems using sparsity enforcing regularization: a case study for the chlorite-iodide reaction, J. Phys. Chem. A 113 (2009) 2775–2785.
[5] Z. An, Q. Hou, Inverse problem in the thick–target method of measurements of inner–shell ionization cross sections by electron or positron impact, Phys. Rev. A 77 (2008) 042702.
[6] P.T. Callaghan, Translational Dynamics and Magnetic Resonance, Oxford University Press, 2011.
[7] J. Keeler, Understanding NMR Spectroscopy, Wiley, second ed., 2010.
[8] M. Fleury, M. Romero-Samiento, Characterization of shales using T_1–T_2 maps, J. Petrol. Sci. Eng. 137 (2016) 55–62.
[9] D. Weber, J. Mitchell, J. McGregor, L.F. Gladden, Comparing strengths of surface interactions for reactants and solvents in porous catalysts using two–dimensional NMR relaxation correlations, J. Phys. Chem. C 113 (2009) 6610–6615.
[10] A.E. English, K.P. Whittall, M.L.G. Joy, R.M. Henkelman, Quantitative two–dimensional time correlation relaxometry, Magnet. Reson. Med. 22 (1991) 425–434.
[11] M.D. Hürlimann, L. Venkataramanan, Quantitative measurement of two–dimensional distribution functions of diffusion and relaxation in grossly inhomogeneous fields, J. Magn. Reson. 157 (2002) 31–42.
[12] Y. Zhang, B. Blümich, Spatially resolved D-T_2 correlation NMR of porous media, J. Magn. Reson. 242 (2014) 41–48.
[13] J.-P. Korb, N. Vorapalawut, B. Nicot, R.G. Bryant, Relation and correlation between NMR relaxation times, diffusion coefficients, and viscosity of heavy crude oils, J. Phys. Chem. C 119 (2015) 24439–24446.
[14] C.L. Lawson, R.J. Hanson, Solving Least Squares Problems, SIAM, 1995.
[15] A.N. Tikhonov, V.Y. Arsenin, Solutions of Ill–posed Problems, V. H. Winston and Sons, 1977.
[16] S.J. Provencher, A constrained regularization method for inverting data represented by linear algebraic or integral equations, Comput. Phys. Commun. 27 (1982) 213–227.
[17] S.J. Provencher, CONTIN: a general purpose constrained regularization program for inverting noisy linear algebraic and integral equations, Comput. Phys. Commun. 27 (1982) 229–242.
[18] G.C. Borgia, R.J.S. Brown, P. Fantazzini, Uniform–penalty inversion of multiexponential decay data, J. Magn. Reson. 122 (1998) 65–77.
[19] L. Ambrosone, A. Ceglie, G. Colafemmina, G. Palazzo, General methods for determining the droplet size distribution in emulsion systems, J. Chem. Phys. 110 (1999) 797–804.
[20] G. Su, X. Zhou, L. Wang, Y. Wang, S. Nie, An inversion method of 2D NMR relaxation spectra in low fields based on LSQR and L–curve, J. Magn. Reson. 265 (2016) 146–152.
[21] P. Babak, S. Kryuchkov, A. Kantzas, Parsimony and goodness–of–fit in multi–dimensional NMR inversion, J. Magn. Reson. 274 (2017) 46–56.
[22] A. Raj, S. Pandya, X. Shen, E. LoCastro, T.D. Nguyen, S.A. Gauthier, Multi–compartment T_2 relaxometry using a spatially constrained multi–Gaussian model, PLoS ONE 9 (2014) e98391.
[23] S. Zheng, Y. Xia, On the measurement of multi-component T_2 relaxation in cartilage by MR spectroscopy and imaging, Magn. Reson. Imaging 28 (2010) 537–545.
[24] Y.-Q. Song, L. Venkataramanan, M.D. Hürlimann, M. Flaum, P. Frulla, C. Straley, T_1–T_2 correlation spectra obtained using a fast two–dimensional Laplace inversion, J. Magn. Reson. 154 (2002) 261–268.
[25] R. Buttgereit, T. Roths, J. Honerkamp, Simultaneous regularization method for the determination of radius distributions from experimental correlation functions, Phys. Rev. E 64 (2001) 041404.
[26] J. Honerkamp, D. Maier, J. Weese, A nonlinear regularization method for the analysis of photon correlation spectroscopy data, J. Chem. Phys. 98 (1993) 865–872.
[27] K.P. Whitall, A.L. MacKay, Quantitative interpretation of NMR relaxation data, J. Magn. Reson. 84 (1989) 134–152.
[28] Y. Song, L. Venkataramanan, L. Burcaw, Determining the resolution of Laplace inversion spectrum, J. Chem. Phys. 122 (2005) 104104.
[29] E.J. Candés, J. Romberg, T. Tao, Robust uncertainty principles: exact signal reconstruction from highly incomplete frequency information, IEEE Trans. Inf. Theory 52 (2006) 489–509.
[30] M. Lustig, D. Donoho, J.M. Pauly, Sparse MRI: the application of compressed sensing for rapid MR imaging, Magn. Reson. Med. 58 (2007) 1182–1195.
[31] M. Benning, L. Gladden, D. Holland, C.-B. Schönlieb, T. Valkonen, Phase reconstruction from velocity–encoded MRI measurements – A survey of sparsity–promoting variational approaches, J. Magn. Reson. 238 (2014) 26–43.
[32] M. Urbańczyk, D. Bernin, W. Koźmiński, K. Kazimierczuk, Iterative thresholding algorithm for multiexponential decay applied to PGSE NMR data, Anal. Chem. 85 (2013) 1828–1833.
[33] R. Bai, D. Benjamini, J. Cheng, P.J. Basser, Fast, accurate 2D–MR relaxation exchange spectroscopy (REXSY): beyond compressed sensing, J. Chem. Phys. 145 (2016) 154202.
[34] G. Gamez, Compressed sensing in spectroscopy for chemical analysis, J. Anal. At. Spectrom. 31 (2016) 2165–2174.
[35] L.I. Rudin, S. Osher, E. Fatemi, Nonlinear total variation based noise removal algorithms, Physica D 60 (1992) 259–268.
[36] D. Benjamini, P.J. Basser, Use of marginal distributions constrained optimization (MADCO) for accelerated 2D MRI relaxometry and diffusometry, J. Magn. Reson. 271 (2016) 40–45.
[37] D. Benjamini, P.J. Basser, Towards clinically feasible relaxation–diffusion MRI using MADCO, Micropor. Mesorpor. Mat. (2017), http://dx.doi.org/10.1016/j.micromeso.2017.02.001.
[38] X. Zhou, G. Su, L. Wang, S. Nie, X. Ge, The inversion of 2D NMR relaxometry data using L_1 regularization, J. Magn. Reson. 275 (2017) 46–54.
[39] T.T. Cai, L. Wang, Orthogonal matching pursuit for sparse signal recovery with noise, IEEE Trans. Inf. Theory 57 (2011) 4680–4688.
[40] M. Burger, M. Möeller, M. Benning, S. Osher, An adaptive inverse scale space method for compressed sensing, Math. Comp. 82 (2013) 269–299.
[41] A. Beck, M. Teboulle, A fast iterative shrinkage–thresholding algorithm for linear inverse problems, SIAM J. Imaging Sci. 2 (2009) 183–202.
[42] K.E. Washburn, P.T. Callaghan, Tracking pore to pore exchange using relaxation exchange spectroscopy, Phys. Rev. Lett. 97 (2006) 175502.
[43] R. Song, Y.-Q. Song, M. Vembusubramanian, J.L. Paulsen, The robust identification of exchange from T_2–T_2 time–domain features, J. Magn. Reson. 265 (2016) 164–171.
[44] P.T. Callaghan, I. Furó, Diffusion-diffusion correlation and exchange as a signature for local order and dynamics, J. Chem. Phys. 120 (2004) 4032–4038.
[45] J.L. Paulsen, Y.-Q. Song, Two–dimensional diffusion time correlation experiment using a single direction gradient, J. Magn. Reson. 244 (2014) 6–11.
[46] K.F. Morris, C.S. Johnson, Resolution of discrete and continuous molecular size distributions by means of diffusion-ordered 2D NMR spectroscopy, J. Am. Chem. Soc. 115 (1993) 4291–4299.

[47] E.L. Cussler, Diffusion: Mass Transfer in Fluid Systems, Cambridge University Press, third ed., 2009.
[48] S. Godefroy, J.-P. Korb, M. Fleury, R.G. Bryan, Surface nuclear magnetic relaxation and dynamics of water and oil in macroporous media, Phys. Rev. E 64 (2001) 021605.
[49] J. Mitchell, T.C. Chandrasekera, L.F. Gladden, Numerical estimation of relaxation and diffusion distributions in two dimensions, Prog. Nucl. Magn. Reson. Spectrosc. 62 (2012) 34–50.
[50] G.H. Golub, C.F. van Loan, Matrix Computations, The John Hopkins University Press, third ed., 1996.
[51] R.G. Baraniuk, Compressive sensing, IEEE Signal Process. Mag. July, 2007, 118–124.
[52] S. Boyd, L. Vandenberghe, Convex Optimization, Cambridge University Press, 2004.
[53] A. Chambolle, T. Pock, A first–order primal-dual algorithm for convex problems with applications to imaging, J. Math. Imaging Vis. 40 (2011) 120–145.
[54] H.Y. Carr, E.M. Purcell, Effects of diffusion on free precession in Nuclear Magnetic Resonance experiments, Phys. Rev. 94 (1954) 630–638.
[55] S. Meiboom, D. Gill, Modified spin-echo method for measuring nuclear relaxation times, Rev. Sci. Instrum. 29 (1958) 688–691.
[56] J.A. Aguilar, M. Nilsson, G. Bodenhausen, G.A. Morris, Spin echo NMR spectra without J modulation, Chem. Commun. 48 (2012) 811–813.
[57] E.L. Hahn, An accurate Nuclear Magnetic Resonance method for measuring spin–lattice relaxation times, Phys. Rev. 76 (1949) 145–146.
[58] J.E. Tanner, Use of the stimulated echo in NMR diffusion studies, J. Chem. Phys. 52 (1970) 2523–2526.
[59] L. Venkataramanan, Y.-Q. Song, M.D. Hürlimann, Solving Fredholm integrals of the first kind with tensor product structure in 2 and 2.5 dimensions, IEEE Trans. Signal Process. 50 (2002) 1017–1026.
[60] G.H. Golub, M. Heath, G. Wahba, Generalized cross–validation as a method for choosing a good ridge parameter, Technometrics 21 (1979) 215–223.
[61] R.J. Gray, Flexible methods for analyzing survival data using splines, with applications to breast cancer prognosis, J. Am. Statist. Assoc. 87 (1992) 942–951.
[62] R. Tibshirani, Regression shrinkage and selection via the Lasso, J. R. Statist. Soc. B 58 (1996) 267–288.
[63] H. Zou, T. Hastie, R. Tibshirani, On the "degrees of freedom" of the Lasso, Ann. Statist. 35 (2007) 2173–2192.
[64] R.J. Tibshirani, J. Taylor, Degrees of freedom in Lasso problems, Ann. Statist. 40 (2012) 1198–1232.
[65] C. Dossal, M. Kachour, M.J. Fadili, G. Peyré, C. Chesnau, The degrees of freedom of the Lasso for general design matrix, Stat. Sinica 23 (2013) 809–828.
[66] H. Akaike, A new look at the statistical model identification, IEEE Trans. Autom. Control 19 (1974) 716–723.
[67] G. Schwarz, Estimating the dimension of a model, Ann. Statist. 6 (1978) 461–464.
[68] C.L. Mallows, Somme comments on C_p, Technometrics 15 (1973) 661–675.
[69] P.C. Hansen, Analysis of discrete ill–posed problems by means of the L–curve, SIAM Rev. 34 (1992) 561–580.
[70] J.N. Tehrani, A. McEwan, C. Jin, A. van Schaik, L_1 regularization method in electrical impedance tomography by using the L_1–curve (Pareto frontier curve), Appl. Math. Model. 36 (2012) 1095–1105.
[71] V.A. Morozov, Methods for Solving Incorrectly Posed Problems, Springer-Verlag, 1984.
[72] J.P. Norton, An Introduction to Identification, Academic Press, 1986.
[73] B. Babadi, N. Kalouptsidis, V. Tarokh, Asymptotic achievability of the Cramér-Rao bound for noisy compressive sampling, IEEE Trans. Signal Process. 57 (2009) 1233–1236.
[74] P.J. Bickel, Y. Ritov, A.B. Tsybakov, Simultaneous analysis of Lasso and Dantzig selector, Ann. Stat. 37 (2009) 1705–1732.
[75] Z. Ben-Haim, Y.C. Eldar, The Cramér-Rao bound for estimating a sparse parameter vector, IEEE Trans. Signal Process. 58 (2010) 3384–3389.
[76] Z. Ben-Haim, Y.C. Eldar, M. Elad, Coherence-based performance guarantees for estimating a sparse vector under random noise, IEEE Trans. Signal Process. 58 (2010) 5030–5043.
[77] P.T. Callaghan, Principles of Nuclear Magnetic Resonance, Oxford University Press, 1991.
[78] D.E. Freed, L. Burcaw, Y.-Q. Song, Scaling laws for diffusion coefficients in mixtures of alkanes, Phys. Rev. Lett. 94 (2005) 067602.
[79] D.E. Freed, Dependence on chain length of NMR relaxation times in mixtures of alkanes, J. Chem. Phys. 126 (2007) 174502.